Multiscale Modeling and Simulation of Water and Methane Hydrate Crystal Interface

*Sina Mirzaeifard, Phillip Servio, Alejandro D. Rey**

Department of Chemical Engineering, McGill University, Montreal H3A 0C5, Canada

Keywords: water-methane hydrate interface; surface physics; interfacial tension; molecular dynamics simulation; NP_NAT ensemble.

ABSTRACT: Water-methane hydrate interfaces are ubiquitous in oil and gas technologies and in Nature. The structure and properties of this liquid/crystal interface plays a significant role in transport phenomena between the bulk phases. In this paper, we use molecular dynamics technique to characterize the liquid water-crystalline methane hydrate in the bulk, and particularly, the interface. We show that the interfacial mechanical approach based on the novel constant normal pressure-cross-sectional area (NP_NAT) ensemble with a computational slab length equal to the lattice parameter of the methane clathrates can accurately predict the interfacial free energy of a curved interface. Notably, the computational platform for the interfacial tension characterization includes contributions from elastic strains. In the studied temperature and pressure ranges, we find that the interfacial tension slightly increases with temperature upturn or pressure drop due to less disordered orientation and dispersed distribution of the molecules at the interface. We generate a full molecular-level characterization by computing the excess enthalpy and stress, local density

profile, radial distribution function, hydrogen bonding density, and charge distribution to confirm the observed interfacial tension trend, which significantly contributes to the evolving understanding of gas hydrate formation.

INTRODUCTION

Under favorable thermodynamic conditions, of low temperature and high pressure, water and gas molecules from a crystalline guest-host solid material known as clathrate or gas hydrate, where the water forms an ordered hydrogen-bonded network that encapsulates the guest gas.[1] These clathrates can form several crystalline structures depending on the size and properties of the encapsulated gas molecules, including sI,[2] sII,[3,4] and sH.[5] In this work, we focus on methane gas as the trapped guest molecule in water cavities forming the sI hydrate phase since the methane hydrate is the most common and important gas hydrates.[6,7]

A fundamental understanding of hydrate nucleation forms the basis to control their formation by inhibition or promotion processes. Based on the application of classical nucleation theory (CNT) to elucidate clathrate formation,[1,8-10] , a complete knowledge of the interfacial energy contributions between all the involved phases, including the hydrate-liquid is critically needed but currently poorly understood.[11,12] According to CNT, the formation work is the sum of a spontaneously driven supersaturation and a surface energy contribution:[13]

$$W(J) = -n\Delta\mu + c(nv_h)^{\frac{2}{3}}\sigma \tag{1}$$

where n, $\Delta\mu(J)$, c, v_h (m^3), and σ (J/m^2) represent the crystal unit cell number, chemical potential difference (supersaturation), shape factor, hydrate volume, and surface energy, respectively. Figure 1 shows representative examples of the water-hydrate interactions in different morphologies,[14] depending on many factors such as the involved phases[15] and fluid flow.[16-18]

Undeniably, there exists a need for extensive characterization of the interfacial tension at the liquid water-clathrate interface, which is shared among all the formation processes. The distribution of hydrate in nature emphasizes the prominence of surface energy, which dictates the optimal morphology and location in the hydrate formation process and its growth rate underlying the Gibbs–Duhem equation.[15] The interfacial tension extensively contributes in the total free energy owing to the normally large surface area engaged in the hydrate systems. The aggregation of hydrate particles is a function of this hydrate-water interfacial tension. A better understanding of interfacial phenomena facilitates the control of the macroscopic behavior of hydrate solutions in nature and technologies in the energy industries based on hydrates. For instance, we may inhibit the hydrate formation in both unconventional and traditional fuel production systems by adsorbing surfactant obtained from synthetic and natural sources.[15] In addition to the formation process, the phase transitions and thermodynamic stability are regulated by the interfacial properties influenced by molecular interactions and structure, which highlights the great importance of surface investigations.[1,15,19,20]

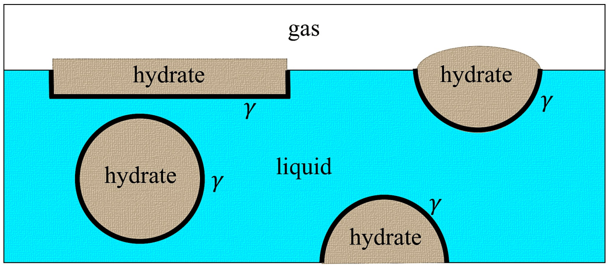

Figure 1. Schematic of water/hydrate interfaces under different nucleation conditions. γ denotes the interfacial tension of this interface.

The mixture of sI methane hydrate in direct contact with liquid water can have significant implications in flow assurance (i.e., management of fluid transportation in multiphase flow), clean energy resources, gas storage and transportation, climate change, environmental processes, and reservoirs associated with the petroleum industries.[21-26] In all these applications, interfacial transport phenomena and thermodynamics, are essential for process control and simulation[27-29] Nevertheless, the characterization and molecular-level understanding are precluded without inputs from simulation.[30,31] Hence, a combination of the analytical theory with numerical computation on the interface between the water and methane hydrate forms the main scope of this work. However, molecular simulations have their own computational challenges in capturing the thermodynamics and physics of the liquid-crystal interfaces due to factors such as sudden density change, unrealistic fluctuations, hydrogen and ion bonding, and adequate time and length scales to obtain sensible results.[32,33] In this work we use specifically tailored molecular dynamic (MD) techniques combined with sophisticated analytical theory to investigate the thermodynamic and mechanic parameters at the bulk and interface as a function of temperature and pressure in both microscopic and macroscopic scales.

Since the water-methane hydrate mixture displays chemical and structural asymmetry and mechanical anisotropy across the interface, we must tackle this system with an appropriate statistical ensemble to predict accurate results. Therefore, we employ the unique NP_NAT ensemble to constrain and control the cross-sectional area (A) and the perpendicular pressure (normal stress component) imposed on the interface (P_N) inspired by its application in the other systems with anisotropic interfaces[34-36] including the liquid-solid mixtures.[37]

In this computational study, we use the well-known mechanical definition of the interfacial tension over the thermodynamic approach,[38-41] although we acknowledge that both local and global perspectives can yield high accuracy.[41,42] The only issue for the mechanical approach is that it is generally applicable to infinite, non-planar (curved) interfaces.[41,43] Here, we demonstrate that we may remarkably overcome these issues allowing us to generate accurate results using a proper MD ensemble and slab length along with an interfacial energy term correction discussed below. To capture the interfacial tension at the desired interface, we require a complete knowledge of the stress tensor which governs the mechanics of the interface. Hence, we follow the Kirkwood and Buff method to obtain all the local components of the tensorial pressure at the water-methane hydrate interface.[40] Additionally, since the mixture interface interpolates a liquid on one side and a crystal on the other, the elastic deformation of the solid surface might influence the interfacial tension via the addition of a reversible work per interfacial area to elastically stretch the surface. This work represents the surface energy change with strain, and it must be included in all the stress-sensitive interfaces, particularly the crystal or solid surfaces, so that the interfacial tension and free energy of the liquid-crystal mixtures are different.[44-49] We generalize the formula of the interfacial tension to incorporate the elastic deformation energy using the Shuttleworth equation.[50-53] In particular we demonstrate the need and importance of this elastic correction to the interfacial tension in the field of gas hydrates.

In addition, we seek to understand how this interfacial tension behaves while being subjected pressure and temperature changes. To the best of our knowledge, this is the first work that reports the interfacial tension at a wide range of practical temperatures and pressures considering the elastic deformation of the crystalline methane hydrate at the interface. Furthermore, this study explains how the molecular orientation, hydrogen bonding network, charge distribution, and local mass density at the interface relate to the interfacial tension.

The organization of this work is as follows. In the following section, we present the modeling and MD simulation details in conjunction with the computational approach for the interfacial tension. In the next section, we report the pressure and temperature effects on the local density and potential energy, the lattice parameter effect, interfacial tension, excess enthalpy and entropy, adsorption, radial distribution function, hydrogen bonding density, and charge distribution. Lastly, we conclude the manuscript with the substantial potential impact of the novel results of this study on present and future work of gas hydrates physics and technologies.

METHODOLOGY

Model and Computational Methods.

We confine the methane hydrate phase between two liquid water phases as previously done.[40,54] The crystalline hydrate phase with 100% cage occupancy contains 1,328 methane and 7,636 water molecules surrounded by 5,468 liquid water molecules in a 3D simulation box with the initial size of 48×48×200 Å and periodic boundary conditions. Figure 2 displays an schematic diagram and snapshot sample of a typical initial configuration of this system.[40,54]

In this study, we use the LAMMPS software[55] to simulate the force fields for the methane and water molecules using the united atom optimized potentials for liquid simulations (OPLS-UA)[56] and transferable intermolecular potential with the four points (TIP4P) models,[57] respectively. In addition, we implement the TIP4P-optimized particle-particle particle-mesh (PPPM) method with the force computation accuracy of 10^{-5} devised by Hockney and Eastwood[58, 59] to compute the Coulombic electrostatic interactions. We also apply the Lennard-Jones (LJ) potential with Lorentz-Berthelot mixing rule to account for the intermolecular interactions:

$$U_{LJ}(r) = 4\varepsilon\left[\left(\frac{\sigma}{r}\right)^{12} - \left(\frac{\sigma}{r}\right)^{6}\right] \tag{2}$$

$$\varepsilon_{ij} = \sqrt{\varepsilon_{ii}\varepsilon_{jj}}\ , \sigma_{ij} = \frac{\sigma_{ii}+\sigma_{jj}}{2} \tag{3}$$

where ε, σ, and r represent the LJ potential well depth, the finite distance at zero potential, and the particles distance, respectively, as shown in Figure 2.[56,57] The cut-off distance of both the LJ and

Coulombic electrostatic interactions is chosen to be 12 Å. Moreover, we utilize the Shake algorithm to constrain the water molecules so that the existing bond lengths and angles refrain from any considerable change throughout the simulations.

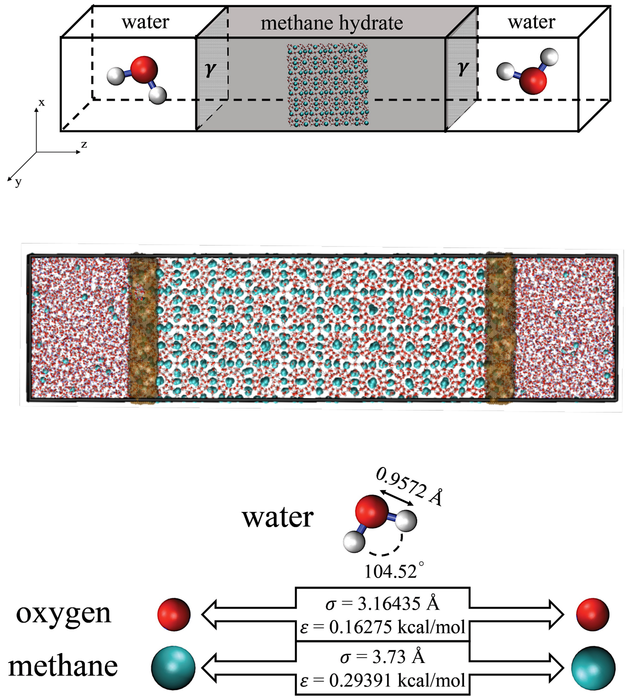

Figure 2. The simulation template showing the red, white, and green particles as the oxygen atom, the hydrogen atom, and the methane molecule, respectively. The brown regions on both sides denote the interfacial zones, which separate the liquid and crystal phases.

We choose a time step of 2 fs through the Verlet algorithm to integrate the non-Hamiltonian equations of motion. The applied thermostat and barostat are Nosé-Hoover and Parrinello-Rahman, respectively, to adjust the temperature and pressure of the system using a damping constant of 4 ps for the characteristic fluctuations. Please note that the damping constant must not be undervalued as we may accommodate with large pressure fluctuations in such solid-liquid systems, which adds to the high complexity of the tensorial pressure calculations. To sample the system configurations, we initially run the simulations for 300 ns using the isothermal-isobaric (*NPT*) ensemble to reach the equilibrium and appropriate lattice parameters at each temperature and pressure. We ensure thermodynamic equilibrium by a series of calculations on the correlation factors of mechanical and thermodynamic properties. We further carry out the simulations for 20 ns employing the isothermal-isobaric-isointerface area (NP_NAT) ensemble, which demands a constant normal pressure (P_N) imposed onto an interface with a persistent cross-sectional area (A) to accurately capture the interfacial phenomena. Constraining the normal pressure and contact surface will help to overcome the above-mentioned issue of pressure control in solid mixtures. We analyze and report the data collected from the last 10 ns of the simulation-run to guarantee accurate results.

Interfacial Tension. We calculate the interfacial tension the following equation based on Bakker's method (γ_B):[60]

$$\gamma_B = \frac{1}{2}\int_{-\infty}^{+\infty}\left(P_N - P_T(z)\right) dz \tag{4}$$

where P_N and P_T denote the normal and tangential pressures, respectively. P_N and P_T can be obtained from the stress tensor given the relations below:[61]

$$P_N = P_{zz} = P \ , \ P_T = \frac{1}{2}\left(P_{xx} + P_{yy}\right) \tag{5}$$

If we neglect the tensorial pressure fluctuations, the P_N and P_T are essentially identical along the simulation box apart from the interfaces owing to a substantial drop in the tangential pressure. Please note that eq 4 is an average of the two standing interfaces on both sides of the methane clathrate phase, which enhances accuracy. Furthermore, the interfacial tension for inhomogeneous multicomponent systems requires a long range or tail correction to compensate the underestimated interatomic interactions caused by the truncation error of setting a cut-off distance.[62-64] Blokhuis *et al*. developed the following formula to calculate the correction term:[62]

$$\gamma_{tail} = \int_0^1 \int_{r_c}^{\infty} 12\pi\varepsilon\sigma^6 \Delta\rho_{HL}{}^2 \left(\frac{3s^3-s}{r^3}\right) cot\left(\frac{rs}{t}\right) dsdr \tag{6}$$

where r_c, t, s, and $\Delta\rho_{HL}$ represent the cut-off distance, interfacial thickness, position, and molecular density difference between the hydrate and liquid phases, respectively.

According to the Shuttleworth equation, the interfacial tension is the sum of the interfacial free energy (θ) and the derivative of the interfacial energy with respect to the deformation or strain (τ):[47,49]

$$\gamma = \theta + A\frac{\partial\theta}{\partial A} = (\gamma_B + \gamma_{tail}) + A\frac{\partial(\gamma_B+\gamma_{tail})}{\partial A} \tag{7}$$

We use a combination of adaptive *NPT* and NP_NAT ensembles throughout the simulations to achieve both cross sectional area variation and precise interfacial energy calculation. Whenever possible the fidelity of the methods and predictions are established with experimental data.

RESULTS AND DISCUSSION

The first step is to find the local density profile of the mixture to perform the tail correction (eqn. 6). The local density is influenced more by the system temperature than the pressure. Figure 3 clearly shows that these density values abruptly decrease as we move from the liquid water phase to the crystalline methane clathrate phase. Such decrease coincides with an increase in the local potential energy across the interface as demonstrated in Figure 4. We fit the density profiles by the standard hyperbolic tangent function to obtain the water and methane hydrate density.

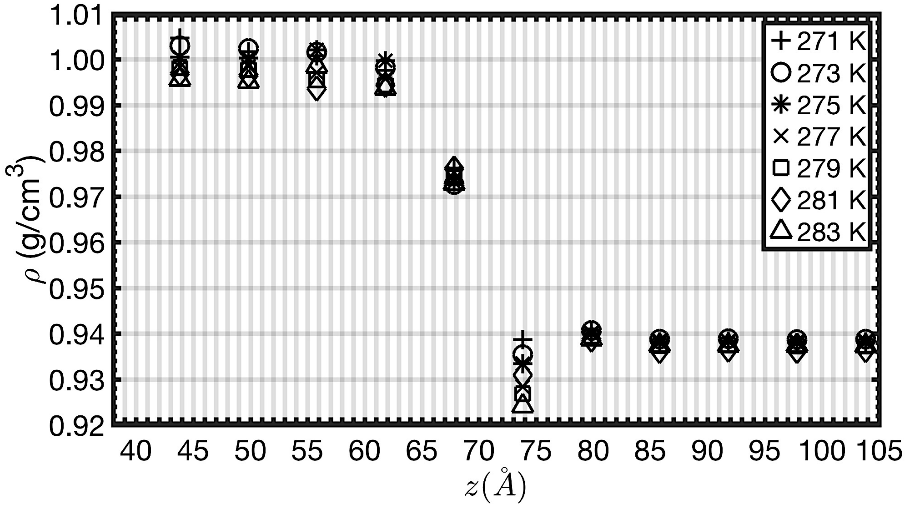

Figure 3. Local density profiles (g/cm³) of the water-methane hydrate mixture along the simulation box at 10 MPa and different temperatures. The plus sign, circle, star, cross, square, diamond, and triangle markers represent the system temperature of 271 K, 273 K, 275 K, 277 K, 279 K, 281 K, and 283 L, respectively.

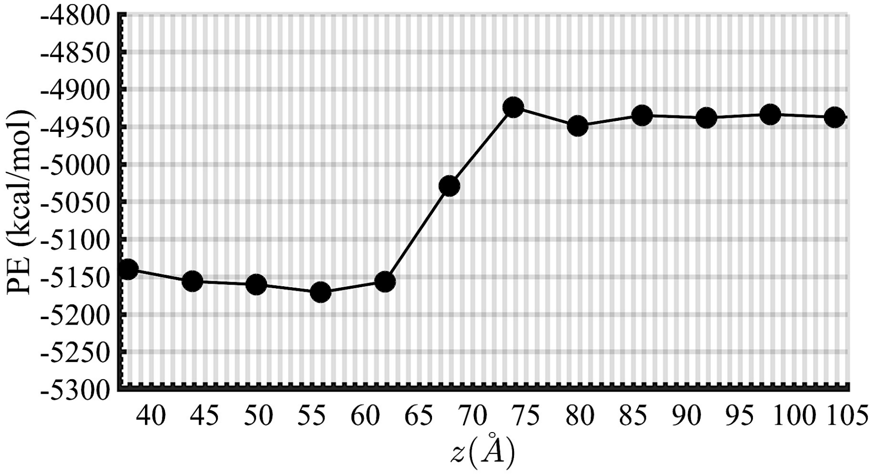

Figure 4. Potential energy (kcal/mol) of the system along the z direction at 10 MPa and 275 K. The potential exhibits a sudden upturn from the liquid water phase to the methane hydrate crystal phase.

We divide the simulation box into several slabs to separately perform the interfacial energy calculation for all slabs. Each slab holds the same planar area in the x- y plane with a constant length along the z direction. This slab length should be carefully chosen to avoid fluctuations in material properties. The appropriate moving average method and slab length are crucial to fully control the pressure of such crystalline solid-liquid mixture; see Figure 5 for representative results on the impact of length scale on pressure's oscillatory behavior. Therefore, we systematically increase the slab length from low to high values and calculate the difference of the normal and tangential pressures, which is critical for the interfacial energy calculation. Figure 6 shows that 12 Å is the shortest length that damps the fluctuation and provides accurate results. Not surprisingly, this length is equal to the lattice parameter of methane hydrate.[1,65] That is why a length of 6 Å, which is half the lattice parameter reveals less fluctuation than 9 Å. This approach allows us to transform a non-planar crystal surface into a planar surface to resolve the issues of the mechanical definition of interfacial tension.

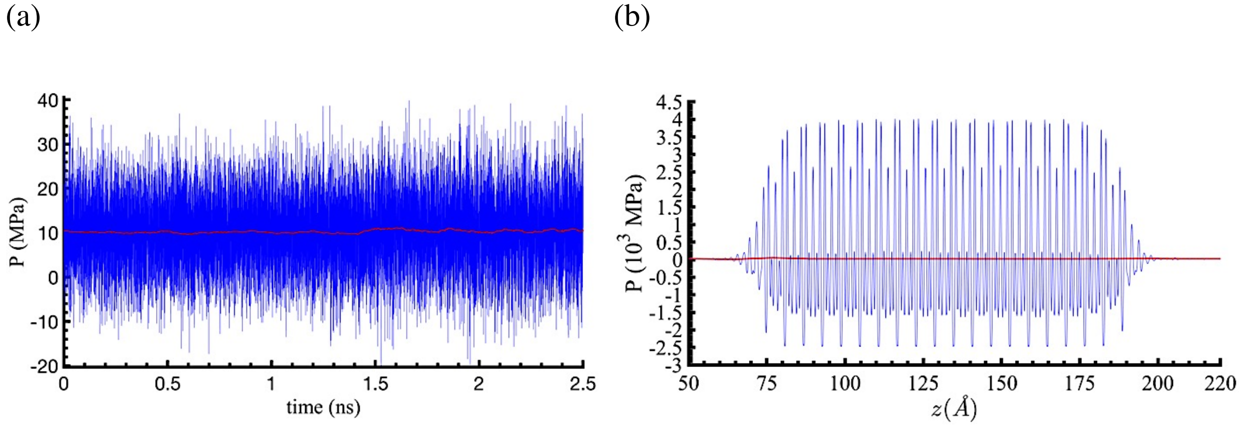

Figure 5. Representative pressure oscillations of the methane hydrate-liquid water mixture at 10 MPa and 275 K. In Figure 5(a), the blue line shows the measured pressure without a damping constant or averaging method. The red line represents the pressure for a system with the use of

sufficient damping constant and moving average method. Figure 5(b) depicts the intense pressure fluctuations when using a short slab length. The blue and red represent the local pressure with the slab length of 0.5 Å and 12 Å, respectively.

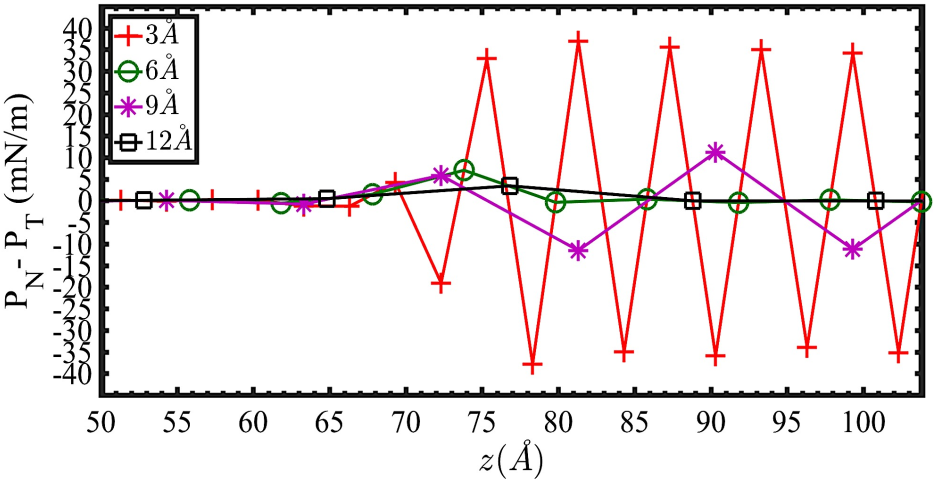

Figure 6. Different slab length changes the difference between the normal and tangential pressures multiplied by the unit length. The temperature of the system is 275 K and the pressure is 10 MPa. Red plus sing, green circle, purple star, and black square markers represent the slab length of 3 Å, 6 Å, 9 Å, and 12 Å, respectively.

With the use of an appropriate slab length, we calculate the interfacial energy and its changes with the elastic deformation. As per eqn. 7, we require these two components to calculate the interfacial tension between the water and methane clathrate phases. Figure 7 shows the interfacial energy decreases as we increase the temperature of the system in a wide range of pressure (5 to 30 MPa). Such a trend for the interfacial energy is observed for the liquid water and methane gas mixtures.[35,38,39,66-68] In contrast to the interfacial energy, the τ contribution increases with the system temperature. The τ values are consistent with the reported results for other crystals and metals.[69] One reasonable explanation is that the temperature rise causes a greater interaction mismatch due to the thermal expansion between the liquid and crystal phases, but the exact calculation of thermal expansion coefficients is beyond the scope of this work. The surface water can be further influenced by the strain as the structure is better ordered than regular liquid water, which could possibly adjust the increase in the lattice and thermal stress which originated from the hydrate phase with temperature increase. This effect understandably corroborates the contribution of the thermal strain in the interfacial tension. Therefore, different pressure regimes at constant temperature reveal a very similar behavior concerning the interfacial crystal elasticity, except for the system with the pressure of 5 MPa because of naturally intense fluctuations in MD simulations of the systems at low pressures.

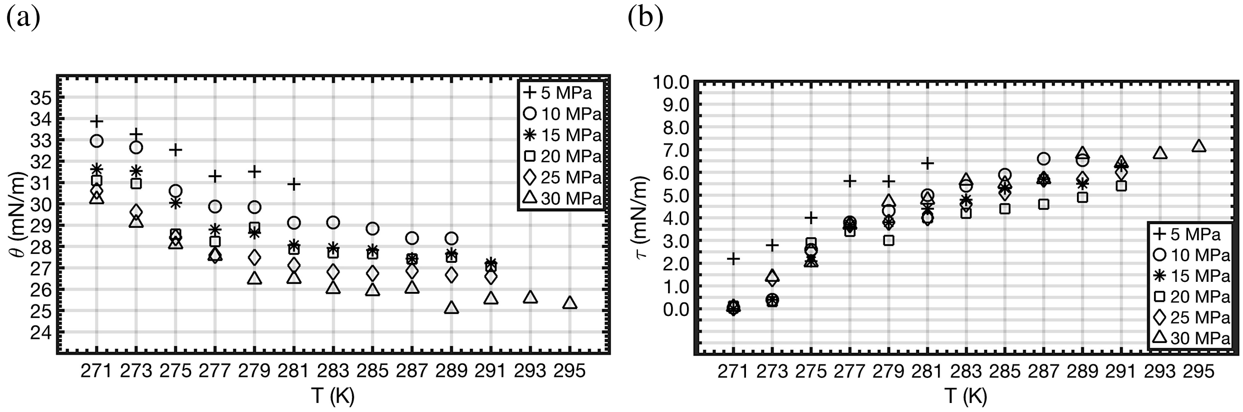

Figure 7. The plot (a) depicts that the interfacial energy decreases with the system temperature at different pressures. Plot (b) shows the variation of the interfacial energy under elastic deformation. The plus sign, circle, star, square, diamond, and triangle markers represent the system pressure of 5 MPa, 10 MPa, 15 MPa, 20 MPa, 25 MPa, and 30 MPa, respectively.

We now combine these two interface and elastic energies terms to obtain the interfacial tension for the systems with systematic increases in the temperature and pressure. Figure 8a evidently exhibits a monotonic increase in interfacial tension of water-methane hydrate mixture with temperature. Such increase in interfacial tension is also observed for other materials such as liquid crystals and ice-water mixtures.[70-77] However, the interfacial tension decreases as the pressure of the system increases following the regular classical behavior until it reaches a plateau due to the very limited compressibility of liquid water and crystalline hydrate (see Figure 8b). These interfacial tension trends with temperature and pressure are also compatible with the surface energy contribution in eqn. 1 since we already know, from thermodynamics, that the hydrates are more likely to form in a high pressure and low temperature regime that imparts a minimum formation work of the surface. Table I presents the interfacial tension values reported in the literature and they are in excellent agreement with those predicted and explained in this work in Figures 8, with approximately a 1.94% deviation. Please note that this deviation is 7.83% when the contribution of the interfacial elastic deformation is neglected.

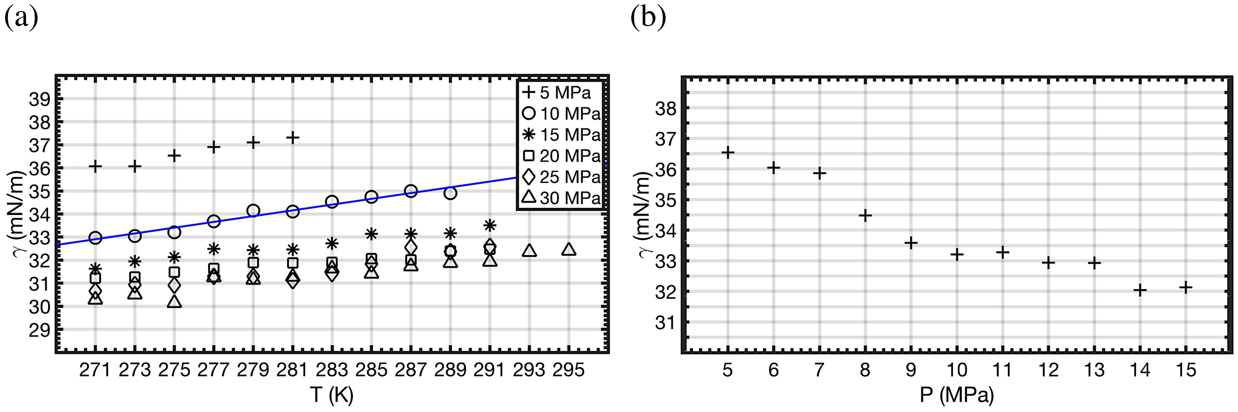

Figure 8. The interfacial tension values (mN/m) for the mixture of water and methane hydrate with increasing system temperature (a) and pressure (b). The plot (b) shows the results of a mixture at 275 K. The plus sign, circle, star, square, diamond, and triangle markers denote the pressure of 5 MPa, 10 MPa, 15 MPa, 20 MPa, 25 MPa, and 30 MPa, respectively. The blue line presents the fitting curve for the system at 10 MPa.

Table 1. Interfacial tension at the water-methane hydrate interface

Investigators	Year	P (MPa)	T (K)	Interfacial tension (mN/m)
Naeiji *et al.*[78]	2017	15	275	31.710
Naeiji *et al.*[78]	2017	20	275	30.776
Jacobson *et al.*[79]	2011	6	275	36±2
Anderson *et al.*[80]	2003	10	275	32±3
Uchida *et al.*[81]	2002	10	275	34±6

Direct numerical simulation (DNS) was utilized in this study to calculate the interface excess enthalpy (H^{ex}) in order to verify the interfacial tension trends with temperature and pressure presented in Figure.8. Figure 9 depicts that the excess enthalpy (H^{ex}) increases with a temperature upturn or with a pressure drop, which is consistent with the interfacial tension increase.

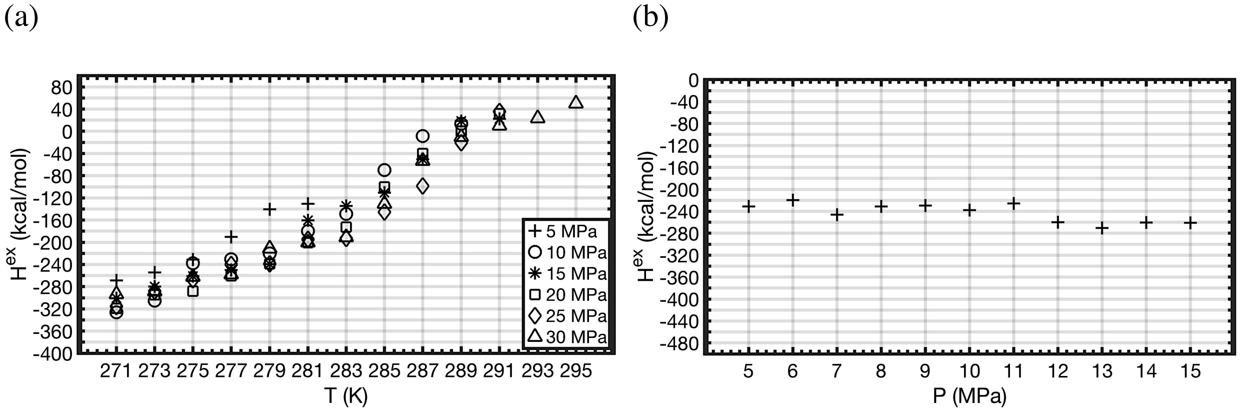

Figure 9. Excess enthalpy (kcal/mol) of the system with systematic change of temperature (a) and pressure (b). The system temperature for the results shown in the plot (b) is 275 K. The excess enthalpy increases as the temperature increases or the pressure decreases. The plus sign,

circle, star, square, diamond, and triangle markers are the system with the pressure of 5 MPa, 10 MPa, 15 MPa, 20 MPa, 25 MPa, and 30 MPa, respectively.

In addition, the excess enthalpy data allow us to calculate the interface excess entropy (S^{ex}) by the thermodynamic relation for Helmholtz free energy:[82]

$$\gamma A = H^{ex} - (PV)^{ex} - TS^{ex} \tag{8}$$

Moreover, we can exploit the fundamental thermodynamic equations and seek more insights into the excess entropy of the mixture in units of kcal/mol using appropriate unit conversions:

$$S^{ex} = -\left(\frac{\partial G}{\partial T}\right)_{A,P} = -\left(\frac{\partial \gamma}{\partial T}\right)_{A,P} \tag{9}$$

Hence, we first fit the interfacial tension data of the mixture at 10 MPa with a linear master curve to report the increasing tension (in units of mN/m):

$$\gamma = 0.12\,T - 0.99 \tag{10}$$

Figure 10 shows the excess entropy values obtained from these two distinct methods deviate by 0.88%, which shows very good agreement between the theory and direct computational thermodynamics. As the system temperature increases, the molecular orientation at the interface becomes less disordered with low fluctuation that consequently weakens the surface entropy and promotes the interfacial tension. Compared to the water bulk phase, the well-ordered water molecules at the interface inhibits the water molecular rotations, which lessens the dielectric constant of the interfacial liquid water adjacent to the crystal surface.[83] Subsequently, this lower water dielectric constant coincides with a tension increase.[84,85] Interestingly, such anomalous behavior does not obey the regular classical entropic effects, which normally shows increase with the temperature.

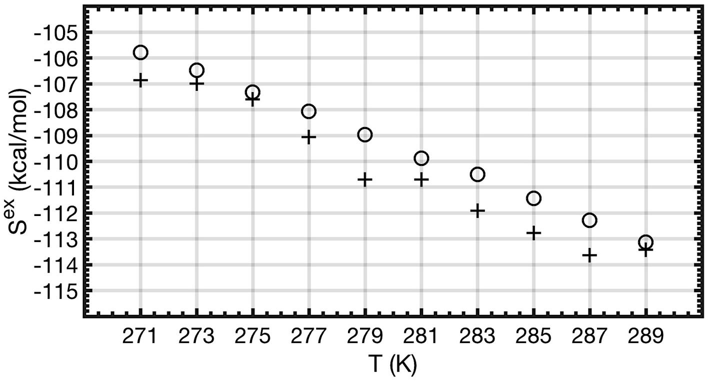

Figure 10. The interfacial excess entropy decreases as the temperature increases. The plus sign and circle markers represent the data obtained from the theory and computational thermodynamics, respectively.

The intermolecular attractions at the interface can suppress the force imbalance leading to the tension decrease. Therefore, an investigation on the interfacial adsorption of the molecules could explain the irregular increase in the interfacial tension with the temperature. Figure 11 depicts that the adsorption of the water molecules onto the water-methane hydrate interface disappears with the temperature increase or pressure decrease. We choose a slab length of 1 Å to obtain an accurate local density profile. The density fluctuations in the right side refer to the crystalline structure of the methane clathrate phase.

Physical van der Waals forces, not chemical interactions, between the guest methane molecules and the host water molecules inside the hydrogen-bonded hydrate cavities provide a sufficiently stable fully-occupied crystalline solid. From a microscopic point of view, the temperature increase at constant pressure leaves the solubility in the hydrate phase unaffected with nearly constant cohesive forces in the bulk, and yet creates larger thermal activity of the water molecules at the interface to disperse the adhesive action, which allows the interfacial tension readily to grow.[86] On the other hand, the increase of system pressure at constant temperature minimizes the tension at the interface by re-arranging the interfacial molecules such that they maximize their contacts inside the surrounding environment.

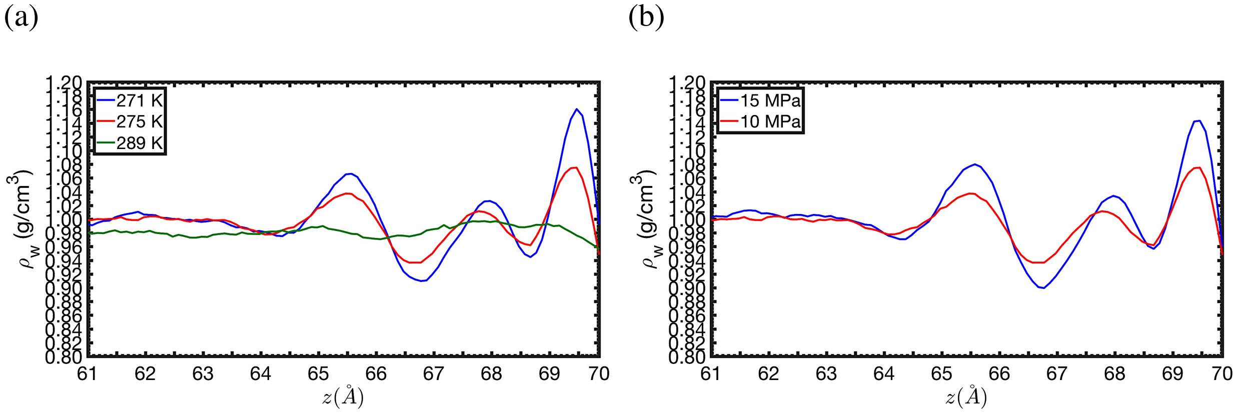

Figure 11. Local density profile of the water molecules demonstrates the interfacial adsorption. The molecular adsorption at the interface vanishes as the temperature increases and the pressure decreases. Please note that the interfacial center exists at z ≈ 66 Å with the liquid water phase on the left and the crystalline methane hydrate phase on the right side. The blue, red, and green lines in the plot (a) represent the system temperature of 271 K, 275 K, and 289 K, respectively, at 10 MPa. The blue and red lines in the plot (b) denote the system pressure of 15 MPa and 10 MPa, respectively, at 275 K.

Next, we report the radial pair distribution function (*g*) to examine the structure of the water molecules in the bulk and the interfacial region. Figure 12a shows that the water molecules become dispersed and disordered as we move from the structured order of the hydrate bulk to the water bulk organization, which is concluded from short and fewer peaks, respectively. This transition influences the interfacial adsorption of the surface water molecules. As well as what has been discussed, Figure 12b represents the interfacial distribution functions between the methane molecules and the oxygen and hydrogen atoms of the water molecules. A higher peak for the oxygen atoms suggests a water molecule orientation with the negative charge towards the methane molecules near the interface.

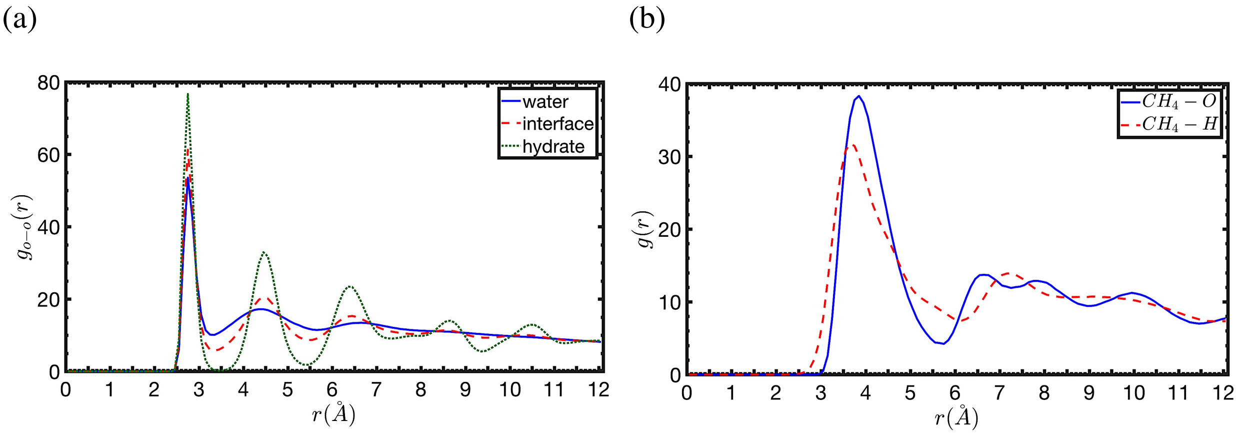

Figure 12. The plot (a) presents the radial pair distribution function between the oxygen atoms in the water bulk (the solid blue line), interface (the dashed red line), and methane hydrate bulk (the dotted green line). The plot (b) shows the radial pair distribution function between the methane molecules and the oxygen atoms (the solid blue line) and the methane molecules and the hydrogen atoms (the dashed red line) at the interface. The temperature and pressure of the mixture are 275 K and 10 MPa.

Additional important insights are gleaned from the hydrogen bonding density near the interface at different temperatures and pressures. We define the distance and angle between the acceptor and donor of the hydrogen bonds subject to constraints. The criterion is that the $O \cdots O - H$ angle and distance between oxygen atoms must be less than 30° and 3.5 Å, respectively. The hydrogen bonding network near the interface might indirectly impact the surface free energy through the interfacial adsorption and the incompatible interaction with the hydrate lattice. A favorable interaction between the hydrogen bonds and the molecules at the interfacial zone leads to the molecular adsorption. In the liquid water-methane gas mixture, a peak in the number of hydrogen bonds has been observed to explain adsorption onto the interface.[35,66,68,87] Conversely, Figure 13 shows a minimum in the hydrogen bond density profile near the interface of the liquid water-methane clathrate mixture at the different temperature and pressure regimes. Temperature increases triggers larger thermal fluctuations at the interface that diminishes the stable hydrogen bonding network, and consequently, its favorable interaction with the bulk water molecules, which leads to less molecular adsorption and higher tension. Furthermore, the interfacial hydrogen bonding seems to be independent of the pressure of the system.

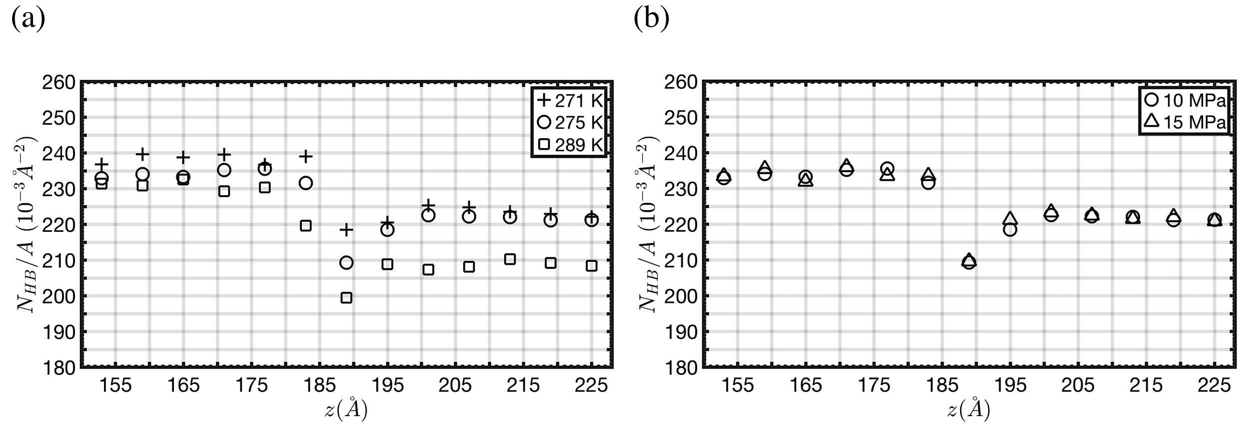

Figure 13. The hydrogen bond density profiles across the simulation box averaged over 1000 configurations at equilibrium at the different system temperature (a) and pressure (b). The interfacial center exists at z ≈ 184 Å with the liquid water phase on the left and the crystalline methane hydrate phase on the right side. In the plot (a), the plus sign, circle, and square markers represent the temperature of 271 K, 275 K, and 289 K, respectively, at 10 MPa. In the plot (b), the circle and triangle markers denote the pressure of 10 MPa and 15 MPa, respectively, at 275 K.

Lastly, we characterize the interfacial polarization charge density to validate the interfacial tension results. Figure 14 clearly demonstrates that a temperature rise or a pressure drop penalizes the interfacial energy by decreasing the interface charge. This reverse proportionality is attributed to the negative electric charge contribution in the tangential pressure tensor component at the interface that has been previously reported.[88-91] The interfacial energy contribution of this unique property can be used to manipulate (i.e., inhibit or promote) the crystal nucleation and growth process via applying an external electric field.[92-94]

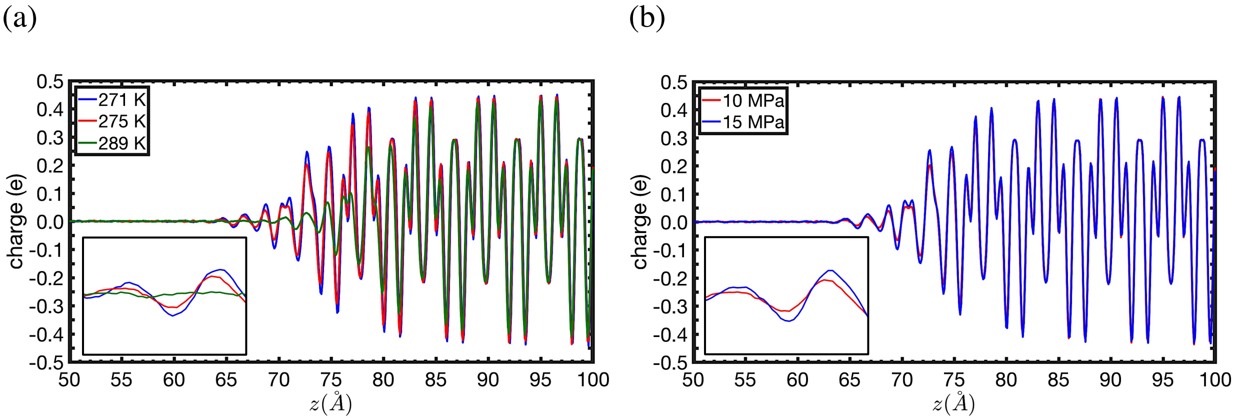

Figure 14. Interfacial charge distribution in units of electron charge at different temperatures (a) and pressures (b). The center of the interface is at z ≈ 66 Å with the water and hydrate phases on the left and right sides, respectively. The blue, red, and green lines in the plot (a) denote the mixtures at 10 MPa and the temperature of 271 K, 275 K, and 289 K, respectively. The red and blue lines in the plot (b) represent the mixtures at 275 K and the pressure of 10 MPa and 15 MPa, respectively. The charge density profiles are enlarged in the insets to better distinguish the lines.

CONCLUSIONS

In the present work, we used molecular dynamics as a computational technique to study the mixture of liquid water and methane hydrate crystal, particularly at the interface. We calculated the potential energy and local density profile of the system at different temperature and pressure to seek the structure-properties relations. The system anisotropy required the application of a novel NP_NAT ensemble and appropriate lattice parameter equal to the methane hydrate lattice parameter to provide an accurate platform for interfacial tension calculations for a non-planar surface, as per the mechanical definition, in order to obtain the most reliable and comprehensive molecular-level information of this important interface. We accounted for a correction based on the Shuttleworth equation to look into the elastic strain contribution to the interfacial tension. The interfacial tension showed slight increase with temperature increase or pressure decrease from 271 K and 30 MPa, respectively, until the melting point pertaining to the methane clathrate-water phase diagram. Such strongly anomalous temperature effect on the interfacial tension defies the standard classical behavior.

In conjunction with the computational approach, we used direct numerical simulation technique to validate the results on the basis of available experimental data. We investigated the excess enthalpy and entropy and concluded that the molecular orientation at the interface become less disordered as the temperature increases. Furthermore, a series of complex calculations on the adsorption, radial pair distribution function, hydrogen bonding density, and charge distribution at the interface generated a full molecular-level characterization and confirmed the interfacial tension variation trend with the system temperature and pressure.

As we increased the temperature or decreased the pressure, the interfacial polarization charge density, minimum number of hydrogen bonding, and intermolecular attractions further perturbed the force balance at the interface, and led to the interfacial tension increase. Furthermore, the interfacial water became less disordered with lower molecular rotation compared to bulk water, which significantly dropped the water dielectric constant near the crystal surface, and subsequently, added to the interfacial tension.

In summary, the results reported provide a sound foundation for the characterization of the water and hydrate interfaces with respect to gas hydrate formation studies. Furthermore, the discussed methods can be extended to the interfacial energy calculations of many industrial, environmental, and biological processes, which deal with the water-crystal mixtures.

AUTHOR INFORMATION

Corresponding Author

*E-mail: alejandro.rey@mcgill.ca. Tel.: +1-514-398-4196. Fax: +1-514-398-6678.

ORCID

Sina Mirzaeifard: 0000-0002-5919-7341

Notes

The authors declare no competing financial interest.

ACKNOWLEDGMENTS

The authors are grateful for the financial support of the Natural Sciences and Engineering Research Council (NSERC), the McGill Engineering Doctoral Awards (MEDA), and the James McGill Professorship appointment. This research is also made possible by the technical and grant support from Compute Canada and Calcul Québec.

REFERENCES

(1) Sloan Jr, E. D.; Koh, C. *Clathrate hydrates of natural gases*; CRC Press, 2007.
(2) Jendi, Z. M.; Servio, P.; Rey, A. D. Ideal strength of methane hydrate and ice Ih from first-principles. *Cryst. Growth Des.* **2015**, *15*, 5301-5309.
(3) Vlasic, T. M.; Servio, P.; Rey, A. D. Atomistic modeling of structure II gas hydrate mechanics: compressibility and equations of state. *AIP Adv.* **2016**, *6*, 085317.
(4) Vlasic, T. M.; Servio, P. D.; Rey, A. D. Effect of guest size on the mechanical properties and molecular structure of gas hydrates from first-principles. *Cryst. Growth Des.* **2017**, *17*, 6407-6416.
(5) Carroll, J. *Natural gas hydrates: a guide for engineers*; Gulf Professional Publishing, 2014.

(6) Demirbas, A. *Methane gas hydrate*; Springer Science & Business Media, 2010.

(7) Klauda, J. B.; Sandler, S. I. Global distribution of methane hydrate in ocean sediment. *Energy Fuels* **2005**, *19*, 459-470.

(8) Bai, X.-M.; Li, M. Test of classical nucleation theory via molecular-dynamics simulation. *J. Chem. Phys.* **2005**, *122*, 224510.

(9) Lupi, L.; Peters, B.; Molinero, V. Pre-ordering of interfacial water in the pathway of heterogeneous ice nucleation does not lead to a two-step crystallization mechanism. *J. Chem. Phys.* **2016**, *145*, 211910.

(10) Warrier, P.; Khan, M. N.; Srivastava, V.; Maupin, C. M.; Koh, C. A. Overview: nucleation of clathrate hydrates. *J. Chem. Phys.* **2016**, *145*, 211705.

(11) Knott, B. C.; Molinero, V.; Doherty, M. F.; Peters, B. Homogeneous nucleation of methane hydrates: unrealistic under realistic conditions. *J. Am. Chem. Soc.* **2012**, *134*, 19544-19547.

(12) Sarupria, S.; Debenedetti, P. G. Homogeneous nucleation of methane hydrate in microsecond molecular dynamics simulations. *J. Phys. Chem. Lett.* **2012**, *3*, 2942-2947.

(13) Kashchiev, D.; Firoozabadi, A. Nucleation of gas hydrates. *J. Cryst. Growth* **2002**, *243*, 476-489.

(14) Kashchiev, D. Nucleation: basic theory with applications; Butterworth Heinemann: Oxford, 2000.

(15) Aman, Z. M.; Koh, C. A. Interfacial phenomena in gas hydrate systems. *Chem. Soc. Rev.* **2016**, *45*, 1678-1690.

(16) Bagherzadeh, S. A.; Englezos, P.; Alavi, S.; Ripmeester, J. A. Influence of hydrated silica surfaces on interfacial water in the presence of clathrate hydrate forming gases. *J. Phys. Chem. C* **2012**, *116*, 24907-24915.

(17) Bai, D.; Chen, G.; Zhang, X.; Sum, A. K.; Wang, W. How properties of solid surfaces modulate the nucleation of gas hydrate. *Sci. Rep.* **2015**, *5*, 12747.

(18) Liang, S.; Kusalik, P. G. The nucleation of gas hydrates near silica surfaces. *Can. J. Chem.* **2014**, *93*, 791-798.

(19) Khadem, S. A.; Rey, A. Theoretical platform for liquid-crystalline self-assembly of collagen-based biomaterials. *Front. Phys.* **2019**, *7*, 88.

(20) Khadem, S. A.; Rey, A. D. Thermodynamic modelling of acidic collagenous solutions: from free energy contributions to phase diagrams. *Soft Matter* **2019**, *15*, 1833-1846.

(21) Sloan, E. D. Fundamental principles and applications of natural gas hydrates. *Nat.* **2003**, *426*, 353-363.

(22) Khadem, S. A.; Boozarjomehry, R. B. Development of systematic framework for an intelligent decision support system in gas transmission network. *Ind. Eng. Chem. Res.* **2015**, *54*, 10768-10786.

(23) Faramawy, S.; Zaki, T.; Sakr, A. E. Natural gas origin, composition, and processing: a review. *J. Nat. Gas Sci. Eng.* **2016**, *34*, 34-54.

(24) Koh, C. A.; Sloan, E. D.; Sum, A. K.; Wu, D. T. Fundamentals and applications of gas hydrates. *Annu. Rev. Chem. Biomol. Eng.* **2011**, *2*, 237-257.

(25) Osborn, S. G.; Vengosh, A.; Warner, N. R.; Jackson, R. B. Methane contamination of drinking water accompanying gas-well drilling and hydraulic fracturing. *Proc. Natl. Acad. Sci.* **2011**, *108*, 8172-8176.

(26) Harriss, R. C.; Sebacher, D. I.; Bartlett, K. B.; Bartlett, D. S.; Crill, P. M. Sources of atmospheric methane in the south Florida environment. *Global Biogeochem. Cycles* **1988**, *2*, 231-243.

(27) Khadem, S. A.; Jahromi, I. R.; Zolghadr, A.; Ayatollahi, S. Pressure and temperature functionality of paraffin-carbon dioxide interfacial tension using genetic programming and dimension analysis (GPDA) method. *J. Nat. Gas Sci. Eng.* **2014**, *20*, 407-413.

(28) Busch, A.; Amann-Hildenbrand, A. Predicting capillarity of mudrocks. *Mar. Pet. Geol.* **2013**, *45*, 208-223.

(29) Nourbakhsh, A., Determination of capillary pressure, relative permeability and pores size distribution characteristics of coal from Sydney basin-Canada. **2012**.

(30) Binks, B. P.; Clint, J. H. Solid wettability from surface energy components: relevance to pickering emulsions. *Langmuir* **2002**, *18*, 1270-1273.

(31) Vázquez, U. O. M.; Shinoda, W.; Moore, P. B.; Chiu, C.; Nielsen, S. O. Calculating the surface tension between a flat solid and a liquid: a theoretical and computer simulation study of three topologically different methods. *J. Math. Chem.* **2009**, *45*, 161-174.

(32) Chaplin, M. Theory vs experiment: what is the surface charge of water? *Water J. Multidiscip. Res.* **2009**, *1*, 1-28.

(33) Eisenberg, D.; Eisenberg, D. S.; Kauzmann, W. *The structure and properties of water*; Oxford University Press on Demand, 2005.

(34) Biscay, F.; Ghoufi, A.; Lachet, V.; Malfreyt, P. Monte Carlo simulations of the pressure dependence of the water– acid gas interfacial tensions. *J. Phys. Chem. B* **2009**, *113*, 14277-14290.

(35) Biscay, F.; Ghoufi, A.; Lachet, V.; Malfreyt, P. Monte Carlo calculation of the methane-water interfacial tension at high pressures. *J. Chem. Phys.* **2009**, *131*, 124707.

(36) Ikeguchi, M. Partial rigid-body dynamics in NPT, NPAT and NPγT ensembles for proteins and membranes. *J. of Comput. Chem.* **2004**, *25*, 529-541.

(37) Noya, E. G.; Vega, C.; de Miguel, E. Determination of the melting point of hard spheres from direct coexistence simulation methods. *J. Chem. Phys.* **2008**, *128*, 154507.

(38) Kvamme, B.; Kuznetsova, T.; Schmidt, K. *In experimental measurements and numerical modelling of interfacial tension in water-methane systems*; Presentation at the International Conference of Computational Methods in Sciences and Engineering, Chania, Greece, 2006.

(39) Schmidt, K. A.; Folas, G. K.; Kvamme, B. Calculation of the interfacial tension of the methane–water system with the linear gradient theory. *Fluid Phase Equilib.* **2007**, *261*, 230-237.

(40) Kirkwood, J. G.; Buff, F. P. The statistical mechanical theory of surface tension. *J. Chem. Phys.* **1949**, *17*, 338-343.

(41) Bahadur, R.; Russell, L. M. Effect of surface tension from MD simulations on size-dependent deliquescence of NaCl nanoparticles. *Aerosol Sci. Technol.* **2008**, *42*, 369-376.

(42) Ghoufi, A.; Malfreyt, P. Calculation of the surface tension and pressure components from a non-exponential perturbation method of the thermodynamic route. *J. Chem. Phys.* **2012**, *136*, 024104.

(43) Nair, A. R.; Sathian, S. P. A molecular dynamics study to determine the solid-liquid interfacial tension using test area simulation method (TASM). *J. Chem. Phys.* **2012**, *137*, 084702.

(44) Butt, H.-J. r.; Graf, K.; Kappl, M. *Physics and chemistry of interfaces*, 2nd ed.; Wiley-VCH: Weinheim, 2006.

(45) Erbil, H. Y. *Surface chemistry of solid and liquid interfaces*; Blackwell Pub.: Oxford, UK , 2006.

(46) Ibach, H. *Physics of surfaces and interfaces*; Springer: Berlin, 2006.

(47) Soustelle, M. *Thermodynamics of surfaces and capillary systems*; ISTE, Ltd.; John Wiley & Sons: London, UK; Hoboken, NJ, 2016.

(48) Bico, J.; Reyssat, É.; Roman, B. Elastocapillarity: when surface tension deforms elastic solids. *Annu. Rev. Fluid Mech.* **2018**, *50*, 629-659.

(49) Qi, X.; Balankura, T.; Fichthorn, K. A. Theoretical perspectives on the influence of solution-phase additives in shape-controlled nanocrystal synthesis. *J. Phys. Chem. C* **2018**, *122*, 18785-18794.

(50) Hecquet, P. Surface energy and surface stress on vicinals by revisiting the Shuttleworth relation. *Surf. Sci.* **2018**, *670*, 58-67.

(51) Lee, J.-Y.; Punkkinen, M.; Schönecker, S.; Nabi, Z.; Kádas, K.; Zólyomi, V.; Koo, Y.; Hu, Q.-M.; Ahuja, R.; Johansson, B. The surface energy and stress of metals. *Surf. Sci.* **2018**, *674*, 51-68.

(52) Xu, Q.; Style, R. W.; Dufresne, E. R. Surface elastic constants of a soft solid. *Soft Matter* **2018**, *14*, 916-920.

(53) Shuttleworth, R. The surface tension of solids. *Proc. Phys. Soc. Sect. A* **1950**, *63*, 444.

(54) Tolman, R. C. Consideration of the Gibbs theory of surface tension. *J. Chem. Phys.* **1948**, *16*, 758-774.

(55) Plimpton, S. Fast parallel algorithms for short-range molecular dynamics. *J. Comput. Phys.* **1995**, *117*, 1-19.

(56) Jorgensen, W. L.; Madura, J. D.; Swenson, C. J. Optimized intermolecular potential functions for liquid hydrocarbons. *J. Am. Chem. Soc.* **1984**, *106*, 6638-6646.

(57) Horn, H. W.; Swope, W. C.; Pitera, J. W.; Madura, J. D.; Dick, T. J.; Hura, G. L.; Head-Gordon, T. Development of an improved four-site water model for biomolecular simulations: TIP4P-Ew. *J. Chem. Phys.* **2004**, *120*, 9665-9678.

(58) Hockney, R. W.; Eastwood, J. W. *Computer simulation using particles*; CRC Press, 1988.

(59) Isele-Holder, R. E.; Mitchell, W.; Ismail, A. E. Development and application of a particle-particle particle-mesh Ewald method for dispersion interactions. *J. Chem. Phys.* **2012**, *137*, 174107.

(60) Ghiass, M.; Rey, A. D. Interfacial thermodynamics of compressible polymer solutions. *J. Chem. Phys.* **2008**, *128,* 071102.

(61) Rowlinson, J. S.; Widom, B. *Molecular theory of capillarity*; Courier Corporation, 2013.

(62) Blokhuis, E.; Bedeaux, D.; Holcomb, C.; Zollweg, J. Tail corrections to the surface tension of a Lennard-Jones liquid-vapour interface. *Mol. Phys.* **1995**, *85*, 665-669.

(63) Chapela, G. A.; Saville, G.; Thompson, S. M.; Rowlinson, J. S. Computer simulation of a gas–liquid surface. Part 1. *J. Chem. Soc., Faraday Trans. 2* **1977**, *73*, 1133-1144.

(64) Grest, G. S.; Stevens, M. J.; Plimpton, S. J.; Woolf, T. B.; Lehoucq, R. B.; Crozier, P. S.; Ismail, A. E.; Mukherjee, R. M.; Draganescu, A. I. *Substructured multibody molecular dynamics*; Sandia National Laboratories, 2006.

(65) Jendi, Z. M.; Rey, A. D.; Servio, P. Ab initio DFT study of structural and mechanical properties of methane and carbon dioxide hydrates. *Mol. Simul.* **2015**, *41*, 572-579.

(66) Mirzaeifard, S.; Servio, P.; Rey, A. D. Molecular dynamics characterization of temperature and pressure effects on the water-methane interface. *Colloid Interface Sci. Commun.* **2018**, *24*, 75-81.
(67) Sachs, W.; Meyn, V. Pressure and temperature dependence of the surface tension in the system natural gas/water principles of investigation and the first precise experimental data for pure methane/water at 25°C up to 46.8 MPa. *Colloids Surf., A* **1995**, *94*, 291-301.
(68) Sakamaki, R.; Sum, A. K.; Narumi, T.; Ohmura, R.; Yasuoka, K. Thermodynamic properties of methane/water interface predicted by molecular dynamics simulations. *J. Chem. Phys.* **2011**, *134*, 144702.
(69) Cammarata, R. C.; Sieradzki, K. Surface and interface stresses. *Annu. Rev. Mater. Sci.* **1994**, *24*, 215-234.
(70) Ambler, M.; Vorselaars, B.; Allen, M. P.; Quigley, D. Solid–liquid interfacial free energy of ice Ih, ice Ic, and ice 0 within a mono-atomic model of water via the capillary wave method. *J. Chem. Phys.* **2017**, *146*, 074701.
(71) Gránásy, L.; Pusztai, T.; James, P. F. Interfacial properties deduced from nucleation experiments: A Cahn–Hilliard analysis. *J. Chem. Phys.* **2002**, *117*, 6157-6168.
(72) Koop, T.; Murray, B. J. A physically constrained classical description of the homogeneous nucleation of ice in water. *J. Chem. Phys.* **2016**, *145*, 211915.
(73) Němec, T. Estimation of ice–water interfacial energy based on pressure-dependent formulation of classical nucleation theory. *Chem. Phys. Lett.* **2013**, *583*, 64-68.
(74) Wood, G.; Walton, A. Homogeneous nucleation kinetics of ice from water. *J. Appl. Phys.* **1970**, *41*, 3027-3036.
(75) Zhang, Y.; Khodadadi, J. Ice-water interfacial energy between 235.35 and 237.15 K deduced from homogeneous nucleation rate. *Curr. Appl. Phys.* **2016**, *16*, 534-538.
(76) Chandrasekhar, S. *Liquid Crystals*, 2nd ed.; Cambridge University Press, 1992.
(77) Rey, A. D. Modeling the Wilhelmy surface tension method for nematic liquid crystals. *Langmuir* **2000**, *16*, 845-849.
(78) Naeiji, P.; Varaminian, F.; Rahmati, M. Comparison of the thermodynamic, structural and dynamical properties of methane/water and methane/water/hydrate systems using molecular dynamic simulations. *J. Nat. Gas Sci. Eng.* **2017**, *44*, 122-130.
(79) Jacobson, L. C.; Molinero, V. Can amorphous nuclei grow crystalline clathrates? the size and crystallinity of critical clathrate nuclei. *J. Am. Chem. Soc.* **2011**, *133*, 6458-6463.
(80) Anderson, R.; Llamedo, M.; Tohidi, B.; Burgass, R. W. Experimental measurement of methane and carbon dioxide clathrate hydrate equilibria in mesoporous silica. *J. Phys. Chem. B* **2003**, *107*, 3507-3514.
(81) Uchida, T.; Ebinuma, T.; Takeya, S.; Nagao, J.; Narita, H. Effects of pore sizes on dissociation temperatures and pressures of methane, carbon dioxide, and propane hydrates in porous media. *J. Phys. Chem. B* **2002**, *106*, 820-826.
(82) Frolov, T.; Mishin, Y. Temperature dependence of the surface free energy and surface stress: An atomistic calculation for Cu (110). *Phys. Rev. B* **2009**, *79*, 045430.
(83) Fumagalli, L.; Esfandiar, A.; Fabregas, R.; Hu, S.; Ares, P.; Janardanan, A.; Yang, Q.; Radha, m.; Taniguchi, T.; Watanabe, K. Anomalously low dielectric constant of confined water. *Sci.* **2018**, *360*, 1339-1342.
(84) Holmes, C. F. Relation between surface tension and dielectric constant. *J. Am. Chem. Soc.* **1973**, *95*, 1014-1016.

(85) Takeuchi, T. Surface tension and dielectric constant. *Proc. Phys.-Math. Soc. Jpn.* **1920**, *2*, 192-194.
(86) Adamson, A. W.; Gast, A. P. *Physical chemistry of surfaces*, 6th ed.; New York: Wiley, 1997.
(87) Mirzaeifard, S.; Servio, P.; Rey, A. D. Molecular dynamics characterization of the water-methane, ethane, and propane gas mixture interfaces. *Chem. Eng. Sci.* **2019**.
(88) Goodisman, J. Surface tension of a charged and polarized system. *J. Phys. Chem.* **1992**, *96*, 6355-6360.
(89) Jiménez-Ángeles, F.; Firoozabadi, A. Induced charge density and thin liquid film at hydrate/methane gas interfaces. *J. Phys. Chem. C* **2014**, *118*, 26041-26048.
(90) Kunieda, M.; Nakaoka, K.; Liang, Y.; Miranda, C. R.; Ueda, A.; Takahashi, S.; Okabe, H.; Matsuoka, T. Self-accumulation of aromatics at the oil−water interface through weak hydrogen bonding. *J. Am. Chem. Soc.* **2010**, *132*, 18281-18286.
(91) Song, J.; Kim, M. W. Excess charge density and its relationship with surface tension increment at the air− electrolyte solution interface. *J. Phys. Chem. B* **2011**, *115*, 1856-1862.
(92) Luis, D.; Herrera-Hernández, E.; Saint-Martin, H. A theoretical study of the dissociation of the sI methane hydrate induced by an external electric field. *J. Chem. Phys.* **2015**, *143*, 204503.
(93) Yan, J.; Patey, G. Heterogeneous ice nucleation induced by electric fields. *J Phys. Chem. Lett.* **2011**, *2*, 2555-2559.
(94) Yan, J.; Patey, G. Ice nucleation by electric surface fields of varying range and geometry. *J. Chem. Phys.* **2013**, *139*, 144501.